

Ferrovalley Physics in Stacked Bilayer Altermagnetic Systems

Yun-Qin Li,¹ Yu-Ke Zhang,¹ Xin-Le Lu,¹ Ya-Ping Shao,¹ Zhi-qiang Bao,¹ Jun-Ding Zheng,^{1,*} Wen-Yi Tong,^{1,†}
Chun-Gang Duan^{1,2,§}

¹Key Laboratory of Polar Materials and Devices (MOE), School of Physics and Electronic Science and Shanghai Center of Brain-inspired Intelligent Materials and Devices, East China Normal University, Shanghai 200241, China

²Collaborative Innovation Center of Extreme Optics, Shanxi University, Taiyuan, Shanxi 030006, China

As an emerging magnetic phase, altermagnets with compensated magnetic order and non-relativistic spin-splitting have attracted widespread attention. Currently, strain engineering is considered to be an effective method for inducing valley polarization in altermagnets, however, achieving controllable switching of valley polarization is extremely challenging. Herein, combined with tight-binding model and first-principles calculations, we propose that interlayer sliding can be used to successfully induce and effectively manipulate the large valley polarization in altermagnets. Using Fe_2MX_4 ($M = \text{Mo}, \text{W}$; $X = \text{S}, \text{Se}$ or Te) family as examples, we predict that sliding induced ferrovalley states in such systems can exhibit many unique properties, including the linearly optical dichroism that is independent of spin-orbit coupling, and the anomalous valley Hall effect. These findings imply the correlation among spin, valley, layer and optical degrees of freedom that makes altermagnets attractive in spintronics, valleytronics and even their crossing areas.

I. INTRODUCTION

Altermagnets (AMs), an emerging magnetic phase, have compensated magnetic order in real space but exhibit the non-relativistic spin-splitting in the reciprocal space, which are receiving widespread attention and research fervor [1-10]. AMs with novel physical properties, such as the crystal Hall effect, spin currents and torques, and tunneling magnetoresistance, have great potential to lead technological innovations in spintronics fields for the fabrication of high-capacity storage devices [11-15]. Up to now, many AMs have been theoretically predicted and experimentally verified, such as bulk MnTe , RuO_2 and CrSb [16-22]. In addition to charge and spin, the valley degree of freedom in valleytronic materials serves as information carriers and are widely utilized for information encoding or storage [23-26]. Ferrovalley materials with spontaneous valley polarization has been firstly proposed in transition metal dichalcogenides in presence of spin-valley locking [27]. Up to now, many spin-related ferrovalley systems have been predicted, such as FeCl_2 , VClBr and VSiGeP_4 [28-32], encouraging the fusion of valleytronics with spintronics. Very recently, the valley-polarized states have been proposed in AMs, including the $\text{V}_2\text{Se}_2\text{O}$, Cr_2O_2 and $\text{A}(\text{BN})_2$ [33-42], which introduces new members to the ferrovalley family. However, valley polarization (VP) in these AMs is mainly realized by strain engineering [33-42], posing significant challenges for experimental control. In view of this, the discovery of other effective methods to regulate VP in AMs is urgent and challenging.

Previous studies proved that the sliding engineering opens a new chapter in the study of the introduction and manipulation of VP in two-dimensional materials [43-47]. Inspired by these, we predict that the interlayer sliding can also be a practical method to induce and control the valley polarization in AMs in addition to strain engineering. We demonstrate this mechanism via first-principles calculations and tight-binding model analysis in the concrete bilayer Fe_2MX_4 family. In such altermagnetic systems with VP induced by sliding effect, there exist intriguing properties, including the spin-valley locking and the anomalous valley Hall effect. Interestingly, the optical selection rule is found at valleys, which has not been discussed in previously reported AMs systems [33-42], offering a noncontact and nondestructive method to detect the emergence of VP and reversal of its polarity. Our findings realize the modulation of valley degree of freedom in AMs by interlayer sliding engineering, offering new perspectives and possibilities for exploring the potential applications of AMs, and paving the way for the development of advanced multifunctional nanodevices in the crossing fields of spintronics and valleytronics.

II. RESULTS

The fully relaxed Fe_2MX_4 structure with the X-M-X sandwich structure is shown in Fig. 1(a), which possesses the space group of $P-42m$ (No. 111, D_{2d} symmetry), same to that of Cu_2MX_4 and V_2MX_4 monolayers [48-50]. Due to the separation of two metal Fe ions by X ions, there is almost no overlap between the electron clouds of adjacent Fe ions, preventing direct exchange for occurring. In fact, the

*jdzheng@phy.ecnu.edu.cn

†wytong@ee.ecnu.edu.cn

§cgduan@clpm.ecnu.edu.cn

direct exchange of magnetic Fe ions with X ions leads to the indirect exchange interaction between Fe₁ and Fe₂ ions (in Fig. 1(b)). Such superexchange coupling effect between Fe₁ and Fe₂ makes them antiferromagnetic (AFM) aligned, in consistent to the computed AFM magnetic ground state with lowest energy (in Fig. S1). The spin density shows that the *PT* symmetry of magnetization density on the opposite Fe spin sublattices is broken by the crystal arrangement of W and X atoms. Two sublattices are linked by mirror symmetries with respect to Fe-X-Fe plane (σ_d operations), rather than crystal translation or inversion (in Fig. S2). Therefore, Fe₂MX₄ is regarded as a type-I altermagnet [10], where its spin splitting is independent of spin-orbital coupling (SOC). As expected, band structures of Fe₂MX₄ exhibit the noticeable non-relativistic spin splitting (in Figs. 1(c) and S3). Calculations of phonon spectra (in Fig. S4) and elastic coefficients C_{kj} (in Table SII) indicate the dynamic and mechanical stabilities of the Fe₂MX₄ systems, which is in consistent to previous study [51]. Indeed, the Cu₂MX₄ materials with the same structure have been experimentally synthesized [48,49], implying the high probability to fabricate Fe₂MX₄ films.

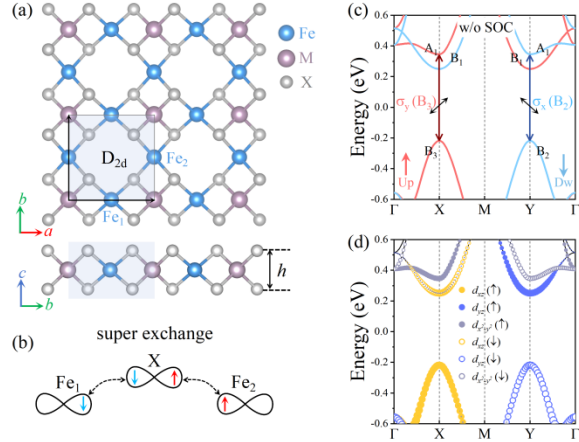


FIG. 1. (a) Top and side views of Fe₂MX₄ monolayers. (b) The superexchange interactions between Fe₁ and Fe₂ atoms via X atoms. (c) Spin-polarized and (d) *d*-orbital projected band structures of Fe atoms in Fe₂WTe₄ monolayer without consideration of SOC. Irreducible representations of bands, *x*- and *y*-polarized lights are marked in (c). The up and down arrows in (d) represent the spin-up and spin-down channels of Fe atoms, respectively.

As shown in Figs. 1(d) and S5, the valence band maximum (VBM) at X and Y valleys is primarily contributed by d_{xz}^\uparrow and d_{yz}^\downarrow orbitals of the Fe₂ and Fe₁ atoms in Fe₂WTe₄. While the conduction band minimum (CBM) at X and Y valleys is contributed by the d_{xz}^\downarrow and d_{yz}^\uparrow of the Fe₁ and Fe₂ atoms. Due to the

prohibition of spin flipping, the optical transition between VBM and CBM at X and Y valleys is forbidden. However, we note that the second conduction band minimum (CBM-2), consisting of $d_{x^2-y^2}$ orbitals, possesses the same spin states as the VBM at a certain valley, making the optical transition between VBM and CBM-2 possible. There exists the spin-valley locking within Fe₂MX₄ system, where the X and Y valleys are locked with spin-up and spin-down channels respectively. According to the great orthogonality theorem, the irreducible representations (IRs) of VBM and CBM-2 meet $B_3 \otimes B_3 = A_1$ in the X valley and $B_2 \otimes B_2 = A_1$ in the Y valley (Details are provided in Supplemental Material (SM)). Such optical selection rule, i.e., the X and Y valleys can independently absorb the *y*- and *x*-polarized light, which hasn't been explored in previous reported altermagnets [33-42]. The imaginary parts of complex dielectric function ϵ_2 of Fe₂MX₄ calculated by our OPTICPACK package [27] are in line with this point. As shown in Fig. S6, absorption edge of *y*- and *x*-polarized light correspond to the energy gap between VBM and CBM-2, proving the prohibition of spin flipping from VBM-CBM hopping. The equivalent energy gap between VBM and CBM-2 in X and Y valleys, along with the degenerated absorption spectra excited by *y*- and *x*-polarized light, demonstrate the paravalley characteristics without spontaneous VP of the pristine Fe₂MX₄. In order to induce VP, strain engineering, which has been adopted in previous valley-related studies of altermagnets [33-41], might be a viable approach. Young's modulus and Poisson's ratio reveal the anisotropic and flexible mechanical properties of Fe₂MX₄ (see Fig. S7), benefiting to modulates physical properties by strains. As shown in Figs. S8 and S9, our calculations of electronic structures and optical spectra prove the effectiveness of inducing VP by uniaxial strain. Nevertheless, controlling VP is still challenging, in demand of switching strain direction between the *x*- and *y*-axis. More effective methods are thus expected to produce and modulate VP.

Sliding engineering is successful in introducing and manipulating VP of multilayers [43-47]. Similar strategy is then employed in Fe₂MX₄ bilayers. Firstly, we build a simplified effective tight-binding (TB) model for Fe₂MX₄ monolayer with D_{2d} point group. We here only consider the d_{xz}^\downarrow , d_{yz}^\downarrow , $d_{x^2-y^2}^\downarrow$ and d_{xz}^\uparrow , d_{yz}^\uparrow , $d_{x^2-y^2}^\uparrow$ for Fe₁ and Fe₂ atoms. The schematic illustration of hopping between lattice sites with the consideration of the nearest-neighbor terms in our TB model is shown in Fig. S10. The hopping interactions between two Fe atoms can be ignored due to their opposite spin states [52], making the zero

values of anti-diagonal terms. The Hamiltonian $H(k)$ for Fe_2MX_4 monolayer can be written as:

$$H(k) = \begin{bmatrix} H^\downarrow(k) & 0 \\ 0 & H^\uparrow(k) \end{bmatrix} \quad (1)$$

$$H^{\downarrow(\uparrow)}(k) = \begin{bmatrix} H_{d_{xz}}^{\downarrow(\uparrow)} & 0 & 0 \\ 0 & H_{d_{yz}}^{\downarrow(\uparrow)} & 0 \\ 0 & 0 & H_{d_{x^2-y^2}}^{\downarrow(\uparrow)} \end{bmatrix} \quad (2)$$

$$H_i^m = \varepsilon_i^m + t_{1i}^m \cos(kx) + t_{2i}^m \cos(ky), \quad (3)$$

$(m = \downarrow, \uparrow; i = d_{xz}, d_{yz}, d_{x^2-y^2})$

where k represents the wave vector, ε and t are on-site energy and hopping parameter, respectively. As shown in Fig. S11, the band structures derived from the Hamiltonian qualitatively rebuild our DFT results for the intrinsic and strained Fe_2MX_4 , which verifies the effectiveness of our six orbitals TB model. We then extend the TB model to Fe_2MX_4 bilayers (in Fig. 2(a)), where the interlayer nearest neighbor hopping is taken into account. The Hamiltonian $H'(k)$ can be written as:

$$H'(k) = \begin{bmatrix} H^{11}(k) & H^{12}(k) \\ H^{21}(k) & H^{22}(k) \end{bmatrix} \quad (4)$$

where the superscripts 1 and 2 represent the bottom and top layers. The Fe_2WX_4 bilayers are intralayer antiferromagnetic and interlayer ferromagnetic couplings, i.e. $H^{11}(k) = H^{22}(k) = H(k)$. Details of TB model is shown in SM. As illustrated in Fig. S12, for the AC_1 (AC_2) state, there is $H^{12}(k) = t'\cos(kx)$ ($H^{12}(k) = t'\cos(ky)$), indicating the breaking of σ_d symmetry (The t' is the hopping between same orbital with same spin in two monolayers). Since all the symmetry operations connecting two valleys are absent, VP state with inequivalent band gap at X and Y valleys is expected to be introduced [46]. In addition, the Hamiltonian of AC_1 and AC_2 states can be regarded as the index exchange between x and y , the sign of VP for these two states should thus be reverted. Switching between AC_1 and AC_2 can be realized through the intermediate AB state. It preserves mirror symmetries along Fe-X-Fe planes, corresponding to the pristine paravalley state without spontaneous VP. Band structures of bilayer Fe_2WX_4 obtained from our TB model (Fig. S12) indicate that interlayer sliding is indeed an effective strategy to introduce and reverse VP through operating σ_d symmetries.

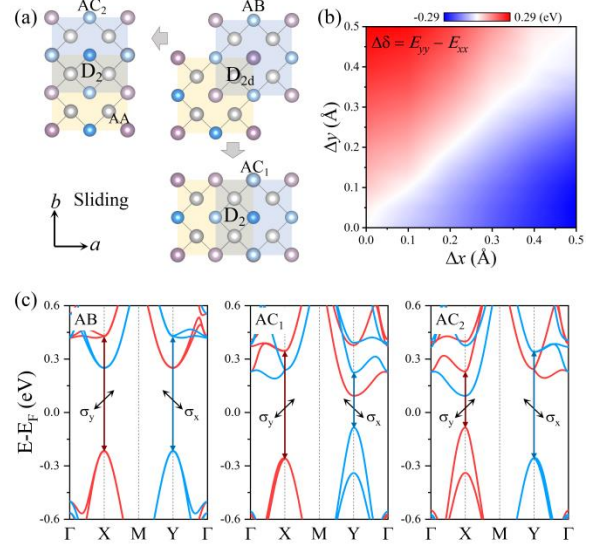


FIG. 2. (a) Schematic structure of a Fe_2MX_4 bilayer with AB, AC_1 and AC_2 stacking orders. (b) Valley polarization difference contour versus $(\Delta x, \Delta y)$ of Fe_2WTe_4 bilayer. Red and blue region represent the optical absorption energy gap of Y valley (E_{xx}) is larger and lower than the X valley (E_{yy}), respectively. (c) Spin-projected band structures without SOC of Fe_2WTe_4 bilayer with AB, AC_1 and AC_2 states.

Following the TB models, we carry out DFT calculations for the Fe_2WTe_4 bilayers. When the top layer slides along the diagonal direction, Fe_2WTe_4 bilayers maintain the D_{2d} symmetry, thus stabilizing in the pristine paravalley state with equivalent absorption edge of y - and x -polarized light (the upper panel of Fig. 3(a)) as the monolayer systems. When the sliding along the x - or y -axis direction occurs, band structures of Fe_2WTe_4 bilayer show inequivalent energy gaps at X and Y valleys (in Fig. 2(c)), corresponding to the ferrovalley state with VP of 0.29 eV (in Fig. 2(b)). Their optical properties own the linear dichroism (in Fig. 3(a)). In the ferrovalley AC_1 state, compared with the spectrum excited by y -polarized light at X valley, the x -polarized one at Y valley experiences a red shift (the middle panel of Fig. 3(a)). When it slides to AC_2 state, as clearly displayed in Fig. 2(c), its VP possess reversed polarity that energy gap in X valley is smaller than the one in Y valley. Following this, in comparison with the y -polarized one, the blue shift of absorption edge related to x -polarized light happens (the bottom panel of Fig. 3(a)). These results indicate that the VP state in Fe_2WTe_4 bilayers can be noncontactively and nondestructively detected by optical methods, promoting the practical utilization of valley degrees of freedom in AMs for information storage and coding.

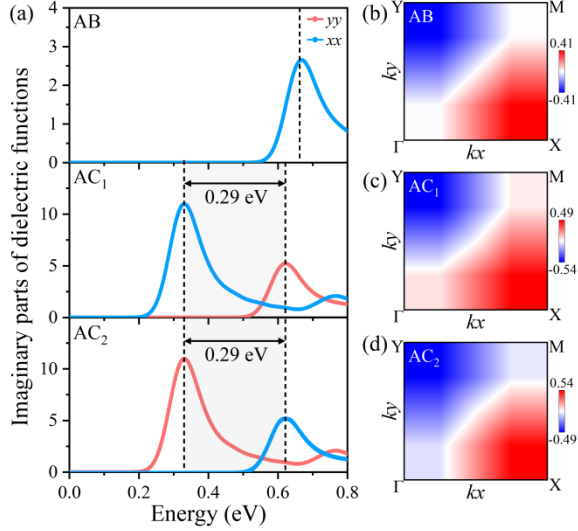


FIG. 3. (a) The imaginary parts of complex dielectric function ϵ_2 and (b-c) Contour maps of Berry curvatures in units of \AA^2 in 2D Brillouin zone in Fe_2WTe_4 bilayers.

Previous analysis in the absence of SOC effect proves that sliding engineering is promising in inducing and manipulating VP of altermagnets. We then explore the effect of SOC on valley physics in Fe_2MX_4 systems. As shown in Figs. S13-S16, the effect of SOC on band dispersion for Fe_2MX_4 monolayer and bilayer systems is negligible, and the optical selection rule is strongly robust against SOC. The presence of SOC may provide interesting phenomena related to Berry curvatures $\Omega(k)$ [27]. We then calculate the $\Omega(k)$ for the VBM in Fe_2MX_4 monolayers and bilayers. For monolayer and AB-stacked bilayer Fe_2WTe_4 that are paravalley states protected by σ_d symmetry, the $\Omega(k)$ around X and Y valleys have opposite sign but identical absolute value $\Omega_z(X) = -\Omega_z(Y)$ (in Figs. 3(b) and S17). The existence of the valley Hall effect, characterized by long-lived spin and valley accumulations, can be expected there. Due to the mirror symmetry breaking in strained monolayers, AC_1 and AC_2 bilayers, the $\Omega(k)$ near X and Y valleys still has opposite sign, but their absolute values are different, indicating the introduction of VP, corresponding to the ferrovalley states. The reversal of VP caused by sliding leads to the inversion of the absolute values of $\Omega(k)$ in X and Y valleys, but their signs remain the same. For the AC_1 state (in Fig. 3(c)), the absolute value of $\Omega(k)$ in Y valley is larger than that of X valley, resulting in a negative summation. When the VP is reversed by sliding to the AC_2 state (in Fig. 3(d)), the summarized $\Omega(k)$ remains the same magnitude yet with opposite sign. Instead of valley Hall effect, the anomalous valley Hall effect (AVHE) exists in these ferrovalley states.

For ferrovalley Fe_2MX_4 bilayers, hole doping shifts the Fermi energy level crossing the top of valence band at Y or X valleys (in Fig. 4(a)). In the p -type AC_1 state (in Fig. 4(b)), the majority carriers, that is, spin-up holes from the Y valley, gain transverse velocities of $v_{\perp} \propto -E \times \Omega_z(k)$ [53,54] towards right side in the presence of external electric field. The accumulation of holes in the right boundary of the ribbon generates a charge Hall current that can be detected as a positive voltage. Conversely, spin-down holes from X valley will accumulate in the left side of ribbons consisting of the AC_2 stacked Fe_2MX_4 bilayer with reversed VP, resulting in a negative transverse charge current. Obviously, Berry curvature serves as an alternative way for determining the emergence of VP and its polarity in AMs. AVHE correlated with it makes the electrically reading and mechanically writing memory devices possible. The binary information is stored by the valley polarization of the ferrovalley Fe_2MX_4 bilayers with the advantage of nonvolatility that could be controlled by sliding through mechanical force. In addition, it can be easily ‘read out’ utilizing the sign of the transverse Hall voltage.

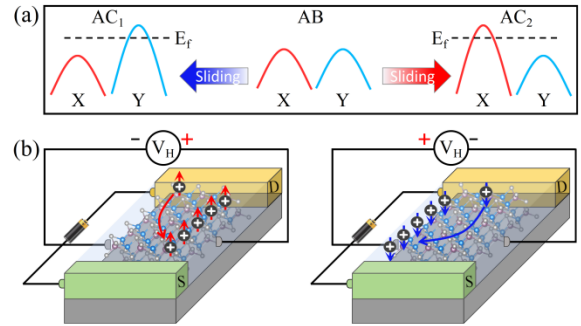


FIG. 4. (a) Sliding induced VP and the Fermi energy levels shift to the top of valence band at Y(X) valleys by holes doping. (b) Diagram of the anomalous valley Hall effect in stacked AC_1 and AC_2 bilayers under holes doping in presence of an in-plane electric field E .

III. CONCLUSIONS

To summarize, based on the combination of the tight-binding model with first-principles calculations, we introduce that sliding engineering is a viable approach to not only induce but also manipulate VP in altermagnets. Taking the Fe_2MX_4 family as representatives, we demonstrate that the ferrovalley states generated by sliding will exhibit a variety of distinctive characteristics, including large VP, linearly optical dichroism and AVHE. We strongly advocate more theoretical and experimental efforts on such an ideal platform to study the interaction among layer, spin, valley, and optical degrees of freedom. It is of great importance in extending the research interest of

altermagnets to valleytronic field and paving the way to their practical applications in the crossing area of spintronics and valleytronics.

ACKNOWLEDGMENTS

This work was supported by the National Key Research and Development Program of China (Grants No. 2022YFA1402902 and No. 2021YFA1200700),

the National Natural Science Foundation of China (Grants No. 12134003 and No. 12304218), National funded postdoctoral researcher program of China (Grant No. GZC20230809), Shanghai Science and Technology Innovation Action Plan (Grant No. 21JC1402000), Shanghai Pujiang Program (Grant No. 23PJ1402200), and East China Normal University Multifunctional Platform for Innovation.

-
- [1] L. Šmejkal, J. Sinova, and T. Jungwirth, Beyond Conventional Ferromagnetism and Antiferromagnetism: A Phase with Nonrelativistic Spin and Crystal Rotation Symmetry. *Phys. Rev. X* **12**, 031042 (2022).
- [2] L. Šmejkal, J. Sinova, and T. Jungwirth, Emerging Research Landscape of Altermagnetism. *Phys. Rev. X* **12**, 040501 (2022).
- [3] Y.-Y. Jiang, Z.-A. Wang, K. Samanta, S.-H. Zhang, R.-C. Xiao, W. J. Lu, Y. P. Sun, E. Y. Tsymlal, and D.-F. Shao, Prediction of giant tunneling magnetoresistance in RuO₂/TiO₂/RuO₂ (110) antiferromagnetic tunnel junctions. *Phys. Rev. B* **108**, 174439 (2023).
- [4] S.-B. Zhang, L.-H. Hu, and T. Neupert, Finite-momentum Cooper pairing in proximitized altermagnets. *Nat. Commun.* **15**, 1801 (2024).
- [5] S. Bhowal and N. A. Spaldin, Ferroically Ordered Magnetic Octupoles in *d*-Wave Altermagnets. *Phys. Rev. X* **14**, 011019 (2024).
- [6] L. Šmejkal, A. H. MacDonald, J. Sinova, S. Nakatsuji, and T. Jungwirth, Anomalous Hall antiferromagnets. *Nat. Rev. Mater.* **7**, 482 (2022).
- [7] R. D. Gonzalez Betancourt *et al.*, Spontaneous Anomalous Hall Effect Arising from an Unconventional Compensated Magnetic Phase in a Semiconductor. *Phys. Rev. Lett.* **130**, 036702 (2023).
- [8] X. Feng *et al.*, Incommensurate Spin Density Wave in Antiferromagnetic RuO₂ Evinced by Abnormal Spin Splitting Torque. *Phys. Rev. Lett.* **132**, 086701 (2024).
- [9] H. Bai *et al.*, Efficient Spin-to-Charge Conversion via Altermagnetic Spin Splitting Effect in Antiferromagnet RuO₂. *Phys. Rev. Lett.* **130**, 216701 (2023).
- [10] S.-W. Cheong and F.-T. Huang, Altermagnetism with non-collinear spins. *npj Quantum Mater.* **9**, 13 (2024).
- [11] L. Šmejkal, R. González-Hernández, T. Jungwirth, and J. Sinova, Crystal time-reversal symmetry breaking and spontaneous Hall effect in collinear antiferromagnets. *Sci. Adv.* **6**, eaaz8809.
- [12] D.-F. Shao *et al.*, Néel Spin Currents in Antiferromagnets. *Phys. Rev. Lett.* **130**, 216702 (2023).
- [13] R. González-Hernández, L. Šmejkal, K. Výborný, Y. Yahagi, J. Sinova, T. Jungwirth, and J. Železný, Efficient Electrical Spin Splitter Based on Nonrelativistic Collinear Antiferromagnetism. *Phys. Rev. Lett.* **126**, 127701 (2021).
- [14] X. Zhou, W. Feng, R.-W. Zhang, L. Šmejkal, J. Sinova, Y. Mokrousov, and Y. Yao, Crystal Thermal Transport in Altermagnetic RuO₂. *Phys. Rev. Lett.* **132**, 056701 (2024).
- [15] O. Fedchenko *et al.*, Observation of time-reversal symmetry breaking in the band structure of altermagnetic RuO₂. *Sci. Adv.* **10**, eadj4883.
- [16] J. Krempaský *et al.*, Altermagnetic lifting of Kramers spin degeneracy. *Nature* **626**, 517 (2024).
- [17] S. Lee *et al.*, Broken Kramers Degeneracy in Altermagnetic MnTe. *Phys. Rev. Lett.* **132**, 036702 (2024).
- [18] T. Osumi, S. Souma, T. Aoyama, K. Yamauchi, A. Honma, K. Nakayama, T. Takahashi, K. Ohgushi, and T. Sato, Observation of a giant band splitting in altermagnetic MnTe. *Phys. Rev. B* **109**, 115102 (2024).
- [19] Y.-P. Zhu *et al.*, Observation of plaid-like spin splitting in a noncoplanar antiferromagnet. *Nature* **626**, 523 (2024).
- [20] S. Reimers *et al.*, Direct observation of altermagnetic band splitting in CrSb thin films. *Nat. Commun.* **15**, 2116 (2024).
- [21] I. J. Park, S. Kwon, and R. K. Lake, Effects of filling, strain, and electric field on the Néel vector in antiferromagnetic CrSb. *Phys. Rev. B* **102**, 224426 (2020).
- [22] Q. Liu, J. Kang, P. Wang, W. Gao, Y. Qi, J. Zhao, and X. Jiang, Inverse Magnetocaloric Effect in Altermagnetic 2D Non-van der Waals FeX (X = S and Se) Semiconductors. *Adv. Funct. Mater.* **n/a**, 2402080 (2024).
- [23] Y.-F. Zhang, H. Guo, Y. Zhu, S. Song, X. Zhang, W. Luo, Y.-Y. Zhang, and S. Du, Emerging Multifunctionality in 2D Ferroelectrics: A Theoretical Review of the Interplay With Magnetism, Valleytronics, Mechanics, and Optics. *Adv. Funct. Mater.* **n/a**, 2410240 (2024).
- [24] J.-D. Zheng, Y.-F. Zhao, Y.-F. Tan, Z. Guan, N. Zhong, F.-Y. Yue, P.-H. Xiang, and C.-G. Duan, Coupling of ferroelectric and valley properties in 2D materials. *J. Appl. Phys.* **132**, 120902 (2022).
- [25] X. Lu, X. Chen, S. Dubey, Q. Yao, W. Li, X. Wang, Q. Xiong, and A. Srivastava, Optical

initialization of a single spin-valley in charged WSe₂ quantum dots. *Nat. Nanotechnol.* **14**, 426 (2019).

[26] S. Shrestha, M. Li, S. Park, X. Tong, D. DiMarzio, and M. Cotlet, Room temperature valley polarization via spin selective charge transfer. *Nat. Commun.* **14**, 5234 (2023).

[27] W.-Y. Tong, S.-J. Gong, X. Wan, and C.-G. Duan, Concepts of ferrovalley material and anomalous valley Hall effect. *Nat. Commun.* **7**, 13612 (2016).

[28] H. Hu, W.-Y. Tong, Y.-H. Shen, X. Wan, and C.-G. Duan, Concepts of the half-valley-metal and quantum anomalous valley Hall effect. *npj Comput. Mater.* **6**, 129 (2020).

[29] Y.-F. Zhao, Y.-H. Shen, H. Hu, W.-Y. Tong, and C.-G. Duan, Combined piezoelectricity and ferrovalley properties in Janus monolayer VCIBr. *Phys. Rev. B* **103**, 115124 (2021).

[30] Y.-Q. Li, X. Zhang, X. Shang, Q.-W. He, D.-S. Tang, X.-C. Wang, and C.-G. Duan, Magnetic and Ferroelectric Manipulation of Valley Physics in Janus Piezoelectric Materials. *Nano Lett.* **23**, 10013 (2023).

[31] W.-Y. Tong and C.-G. Duan, Electrical control of the anomalous valley Hall effect in antiferrovalley bilayers. *npj Quantum Mater.* **2**, 47 (2017).

[32] H. Hu, W.-Y. Tong, Y.-H. Shen, and C.-G. Duan, Electrical control of the valley degree of freedom in 2D ferroelectric/antiferromagnetic heterostructures. *J. Mater. Chem. C* **8**, 8098 (2020).

[33] H.-Y. Ma, M. Hu, N. Li, J. Liu, W. Yao, J.-F. Jia, and J. Liu, Multifunctional antiferromagnetic materials with giant piezomagnetism and noncollinear spin current. *Nat. Commun.* **12**, 2846 (2021).

[34] J. Gong, Y. Wang, Y. Han, Z. Cheng, X. Wang, Z.-M. Yu, and Y. Yao, Hidden Real Topology and Unusual Magnetoelectric Responses in Two-Dimensional Antiferromagnets. *Adv. Mater.* **36**, 2402232 (2024).

[35] Y. Wu, L. Deng, X. Yin, J. Tong, F. Tian, and X. Zhang, Valley-Related Multipiezo Effect and Noncollinear Spin Current in an Altermagnet Fe₂Se₂O Monolayer. *Nano Lett.* (2024).

[36] Y. Zhu, T. Chen, Y. Li, L. Qiao, X. Ma, C. Liu, T. Hu, H. Gao, and W. Ren, Multipiezo Effect in Altermagnetic V₂SeTeO Monolayer. *Nano Lett.* **24**, 472 (2024).

[37] Q. Cui, Y. Zhu, X. Yao, P. Cui, and H. Yang, Giant spin-Hall and tunneling magnetoresistance effects based on a two-dimensional nonrelativistic antiferromagnetic metal. *Phys. Rev. B* **108**, 024410 (2023).

[38] H.-Y. Ma, D. Guan, S. Wang, Y. Li, C. Liu, H. Zheng, and J.-F. Jia, Quantum spin Hall and quantum anomalous Hall states in magnetic Ti₂Te₂O single layer. *J. Phys.: Condens. Matter* **33**, 21LT01 (2021).

[39] P.-J. Guo, Z.-X. Liu, and Z.-Y. Lu, Quantum anomalous hall effect in collinear antiferromagnetism. *npj Comput. Mater.* **9**, 70 (2023).

[40] X. Chen, D. Wang, L. Li, and B. Sanyal, Giant spin-splitting and tunable spin-momentum locked transport in room temperature collinear antiferromagnetic semimetallic CrO monolayer. *Appl. Phys. Lett.* **123**, 022402 (2023).

[41] S.-D. Guo, X.-S. Guo, K. Cheng, K. Wang, and Y. S. Ang, Piezoelectric altermagnetism and spin-valley polarization in Janus monolayer Cr₂SO. *Appl. Phys. Lett.* **123**, 082401 (2023).

[42] R.-W. Zhang, C. Cui, R. Li, J. Duan, L. Li, Z.-M. Yu, and Y. Yao, Predictable Gate-Field Control of Spin in Altermagnets with Spin-Layer Coupling. *Phys. Rev. Lett.* **133**, 056401 (2024).

[43] T. Zhong, Y. Ren, Z. Zhang, J. Gao, and M. Wu, Sliding ferroelectricity in two-dimensional MoA₂N₄ (A = Si or Ge) bilayers: high polarizations and Moiré potentials. *J. Mater. Chem. A* **9**, 19659 (2021).

[44] E. Y. Tsybal, Two-dimensional ferroelectricity by design. *Science* **372**, 1389 (2021).

[45] Y. Wu, J. Tong, L. Deng, F. Luo, F. Tian, G. Qin, and X. Zhang, Coexisting Ferroelectric and Ferrovalley Polarizations in Bilayer Stacked Magnetic Semiconductors. *Nano Lett.* **23**, 6226 (2023).

[46] Y.-K. Zhang *et al.*, Ferroelastically controlled ferrovalley states in stacked bilayer systems with inversion symmetry. *Phys. Rev. B* **108**, L241120 (2023).

[47] G. Yu, J. Ji, C. Xu, and H. J. Xiang, Bilayer stacking ferrovalley materials without breaking time-reversal and spatial-inversion symmetry. *Phys. Rev. B* **109**, 075434 (2024).

[48] C. J. Crossland, P. J. Hickey, and J. S. O. Evans, The synthesis and characterisation of Cu₂MX₄ (M = W or Mo; X = S, Se or S/Se) materials prepared by a solvothermal method. *J. Mater. Chem.* **15**, 3452 (2005).

[49] A. P. Tiwari, A. Azam, T. G. Novak, O. Prakash, and S. Jeon, Chemical strain formation through anion substitution in Cu₂WS₄ for efficient electrocatalysis of water dissociation. *J. Mater. Chem. A* **6**, 7786 (2018).

[50] Y. Jiang, H. Wang, K. Bao, Z. Liu, and J. Wang, Monolayer V₂MX₄: A New Family of Quantum Anomalous Hall Insulators. *Phys. Rev. Lett.* **132**, 106602 (2024).

[51] C.-Y. Tan, Z.-F. Gao, H.-C. Yang, K. Liu, P.-J. Guo, and Z.-Y. Lu, (2024).

[52] W.-Y. Tong, H.-C. Ding, S. J. Gong, X. Wan, and C.-G. Duan, Magnetic ordering induced giant optical property change in tetragonal BiFeO₃. *Sci. Rep.* **5**, 17993 (2015).

[53] X. Feng, C. S. Lau, S.-J. Liang, C. H. Lee, S. A. Yang, and Y. S. Ang, Half-Valley Ohmic Contact:

Contact-Limited Valley-Contrasting Current Injection.
Adv. Funct. Mater. **34**, 2309848 (2024).

[54] Y. Liu, Y. Feng, Y. Dai, B. Huang, and Y. Ma,
Engineering Layertronics in Two-Dimensional
Ferromagnetic Multiferroic Lattice. Nano Lett. **24**,
3507 (2024).